Fast Linear Registration of 3D Objects Segmented from Medical Images

Attila Tanács and Zoltan Kato

Department of Image Processing and Computer Graphics

University of Szeged, Hungary

Abstract—In this paper a linear registration framework is used for medical image registration using segmented binary objects. The method is best suited for problems where the segmentation is available, but we also propose a general bone segmentation approach for CT images. We focus on the case when the objects to be registered differ considerably because of segmentation errors. We check the applicability of the method to bone segmentation of pelvic and thoracic CT images. Comparison is also made against a classical mutual information-based registration method.

I. INTRODUCTION

3D imaging in medical and industrial applications is common nowadays. Taking 3D images of the same or similar objects at different times raises the problem of *registration*, *i.e.* establishing the geometric correspondence between these images. Registration of medical images plays an important role in *e.g.* diagnostics, tumor growth monitoring, treatment planning and surgery execution. Many approaches have been proposed for a wide range of problems in the past decades [1], [2].

An important decision is the type of geometric transformation to consider. Non-linear transformations can be used to *e.g.* model tissue movements and local changes of shapes [3], [4]. These algorithms must take into account the deformation parameters of different tissue types which can be hard, application specific and time consuming task. In many scenarios global linear transformations are sufficient, however, especially if fast registration is necessary.

Intrapatient registrations of the brain [5] and bone structures can be treated as rigid movements. In computer integrated surgery applications computing complexity is usually an important factor; on-line registration may be required for registering pre-operative images to intra-operative ones [6], which may be achievable using rigid deformations. When monitoring tumor growth, rigid registration is usually required since affine or non-linear transformations would make unwanted changes in size. For such tasks, hybrid imaging modalities are especially useful [7], [8]. They produce both morphological (CT) and functional images (PET or SPECT) which are registered. The morphological images then can be used for rigid registration of follow up studies. Affine transformations may be considered for *e.g.* registration of prostate in Radiotherapy Therapy Planning [9], interpatient registration tasks of *e.g.* the brain, generating statistical atlas information from interpatient data, or as a coarse registration step before a non-linear one.

Classical methods solve the registration problem by either extracting *geometric features* or using the *image intensities* directly, and try to establish correspondences by usually applying an iterative technique. Geometric features can be *e.g.* points, surfaces [6] or skeletons [10]. Intensity similarity methods are used mainly for non-binary single- and multi-modality medical registration problems, but can also be applied for registration of binary images [11].

Since the iterative search in these methods uses the features/intensities in each step, they suffer from considerably increased computational complexity in case of large amount of data. Here we utilize a linear registration framework that requires binary objects [12]. Such objects may be created directly by the imaging process (*e.g.* discrete tomography), generated from geometric descriptions (*e.g.* from CAD models), or by segmenting corresponding regions from non-binary images. An easily and efficiently solvable polynomial system of equations is generated by a single pass over the images. No correspondences are required, thus the solution does not depend on the size of the objects. This makes this method especially suitable for registering large volume images.

The method assumes that by applying the optimal transformation the objects become identical. This rarely happens in real registration problems. In this paper we examine the applicability of the method to bone structure registrations of pelvic and thoracic studies.

II. REGISTRATION METHOD

Based on [12], here we briefly summarize the main points of the applied registration framework. Let us denote the object points of the *template* and the *observation* volume images by $\mathbf{x}, \mathbf{y} \in \mathbb{P}^3$, respectively in the projective space. Let $\mathbf{A}$ denote the unknown, non-singular 4×4 homogeneous matrix of the affine transformation that we want to recover. It relates the template and observation as $\mathbf{A}\mathbf{x} = \mathbf{y} \Leftrightarrow \mathbf{x} = \mathbf{A}^{-1}\mathbf{y}$. The above equations still hold when a properly chosen function $\omega : \mathbb{P}^3 \to \mathbb{P}^3$ is acting on both sides of the equations [13]: $\omega(\mathbf{A}\mathbf{x}) = \omega(\mathbf{y}) \quad \Leftrightarrow \quad \omega(\mathbf{x}) = \omega(\mathbf{A}^{-1}\mathbf{y})$. In order to avoid the need for point correspondences, we integrate over the foreground domains $\mathcal{F}_t$ and $\mathcal{F}_o$ of the *template* and the *observation*, respectively, yielding

$$|\mathbf{A}| \int_{\mathcal{F}_t} \omega(\mathbf{x}) \, d\mathbf{x} \quad = \quad \int_{\mathcal{F}_o} \omega(\mathbf{A}^{-1}\mathbf{y}) \, d\mathbf{y} \, . \qquad (1)$$

The Jacobian of the transformation is $|\mathbf{A}| = \int_{\mathcal{F}_o} d\mathbf{y} / \int_{\mathcal{F}_t} d\mathbf{x}$.

We need at least 12 equations since a 3D affine transformation is determined by 12 parameters. Sufficiently many linearly independent equations can be generated by making use of the relation in Eq. (1). We select polynomial ω functions such that their k-th coordinate is of the form $\omega(\mathbf{x})_{f,g,h}^{(k)} = x_1^f \cdot x_2^g \cdot x_3^h$, where $f, g, h \in \mathbb{N}$, $f + g + h = d$, and $d \in \{1, 2, 3\}$. From Eq. (1) these functions generate the following polynomial equations:

$$|\mathbf{A}| \int_{\mathcal{F}_t} x_a \, d\mathbf{x} = \sum_{i=1}^{4} q_{ai} \int_{\mathcal{F}_o} y_i \, d\mathbf{y} , \quad (2)$$

$$|\mathbf{A}| \int_{\mathcal{F}_t} x_a x_b \, d\mathbf{x} = \sum_{i=1}^{4} \sum_{j=1}^{4} q_{ai} q_{bj} \int_{\mathcal{F}_o} y_i y_j \, d\mathbf{y} , \quad (3)$$

$$|\mathbf{A}| \int_{\mathcal{F}_t} x_a x_b x_c \, d\mathbf{x} = \sum_{i=1}^{4} \sum_{j=1}^{4} \sum_{k=1}^{4} q_{ai} q_{bj} q_{ck} \int_{\mathcal{F}_o} y_i y_j y_k \, d\mathbf{y} \quad (4)$$

where $1 \leq a, b, c \leq 3$, $a \leq b \leq c$, and q_{ij} denote the unknown elements of the inverse transformation $\mathbf{A}^{-1}$, yielding 19 equations. In order to increase numerical stability, we add another 19 similar equations by changing the role of the point sets $\mathbf{x}$ and $\mathbf{y}$. Note, that this step introduces no new unknown parameters, since $\mathbf{A}$ is uniquely determined by parameters q_{ij} in the non-singular case. This produces an overdetermined system of equations up to third order.

For discrete digital images the formulations still hold if integrals are interchanged for summation, and the calculation of the Jacobian is approximated by the ratio of the volumes spanned by the objects (*e.g.* voxel counts). The system of such polynomial equations can be efficiently solved using the standard Levenberg-Marquardt (L-M) method. The iterative L-M solution makes it possible to impose restrictions on the transformation to be found, producing rigid-body or similarity transformations instead of affine. This can be achieved by *e.g.* selecting the 6 parameters of the rigid-body transformation for use by the solver, while from these 6 parameters the 4×4 affine matrix is computable when calculating the error of the system of polynomial equations[1].

Notice that all unknowns are outside of the integrals in Eq. (2), thus the integrals have to be evaluated only once. Its time complexity is $\mathcal{O}(N)$, where N is the number of the voxels of the object, since all the summations can be computed in a single pass over the volume image.

Since L-M is an iterative process, we found that the solution is sensitive to the initial start position. Rotation was found to be the main problem, thus we systematically started the search from 27 different orientations corresponding to 120 degrees of rotation along each axes, and used heuristics to earlier termination of non-promising directions. Note that this search strategy is not necessary if the orientations of the objects are closer than 120 degrees, which is generally fulfilled with CT imaging.

---

[1]Note that the Jacobian is 1 for rigid-body transformations. Since in real registration problems the identity criterion is not fulfilled, we got better results using the approximated value of the Jacobian instead of 1.

III. MEDICAL APPLICATIONS

Fast rigid-body registration of bone structures is important in image guided surgical planning in execution for registering pre-operative volumes to intra-operative ones. Zhang *et al.* give an overview of surface based registration techniques [6] and propose a 15 times faster method than standard Iterative Closest Point (ICP) methods. However, it still takes around one minute to register vertebrae models segmented from high resolution CT images. If the segmentation is available, our method could be used instead of ICP to get the result faster.

Affine registration is also applied for creation of brain atlases, at least as preliminary step before an elastic or non-linear part [14]. Automatic initial placement of deformable organ models can also benefit from fast linear registrations [15]. By collecting and transforming a set of images to a common reference frame, a probabilistic atlas can be produced for various organs. Using the same registration method, this probabilistic atlas data can be mapped to the space of the study to be segmented. Here precise alignment of all anatomical structures is not crucial, the focus is on fast execution.

In [16], Ma *et al.* propose a similar approach to ours for registration of serial sections of microscope images. After a binarization step, an initial rigid transformation is computed based on the centroids (translation) and moments (rotation) of the binary objects. Then a correlation-based iterative technique is applied that optimizes the overlap between the objects. It takes around 6 seconds to register one 2D section pairs. Our more sophisticated method could replace the first step.

Rigid registration of thoracic images are also applicable for *e.g.* lymphoma detections and changes over time using PET-CT scanners. PET images delineate the uptake of the contrast agent in organs (lymph nodes), while the CT modality can be used for registration and morphological localization. Here non-rigid registrations are discouraged since these could change the size of the organs.

A. Segmentation

Since our method is based on binary objects, we have to extract such information from the images. Our registration algorithm is best suited for tasks where such information is readily available, which is the case in several tasks. Otherwise, bone structures are usually relatively easy to extract from CT images in acceptable quality for our method. Here we propose a general framework for segmentation. This approach is able to remove the high intensity parts of the bed from below the patient and other high intensity tissue regions that are not bones (*e.g.* the parts of the colon delineated in the bone intensity range, if they do not touch the bone).

Algorithm 1 summarizes the main steps, while Fig. 1 shows the results of Steps 3, 4 and 9. In Step 2, we have to set a threshold value to produce a binary image. Since bone structures have high intensity values in CT images, we set it to keep the upper 20% of the image intensity interval. Step 3 is for removing noise artifacts; these usually are of small size. Experimentally we set this threshold to 40 mm^2. It is
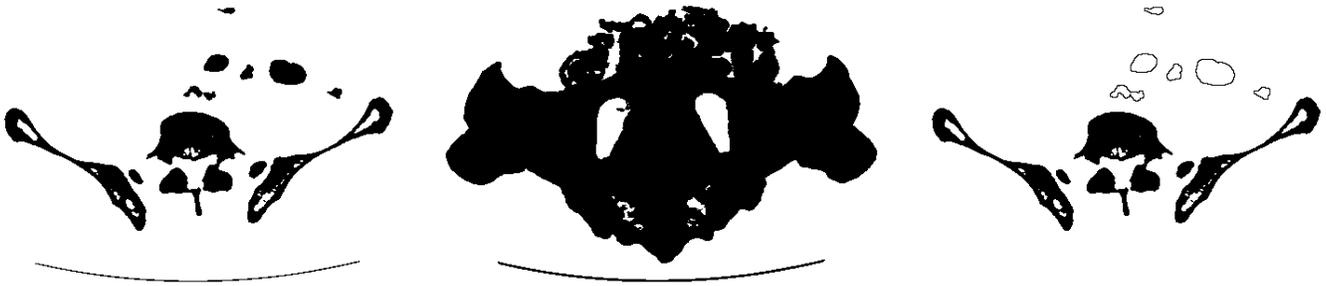
Fig. 1. Segmentation of a pelvic CT image (only a 2D slice of a 3D volume is shown). *Top*: The image is binarized and the small connected objects are removed as the result of Step 3. *Middle*: Slices are projected along the Z-axis in Step 4. By keeping the largest connected region, it is possible to remove the bed from the image. *Bottom*: Objects that fall outside of the largest connected component of the dilated image are detected as outliers (blobs shown with outline only). Notice that even small bone regions are correctly classified.

advisable to select only those 2D slices of the volumes that delineate roughly the same parts of the body.

Algorithm 1: Bone segmentation from a CT image

Input: CT study
Output: "Bone", "outlier", "other object" classification of voxels

1 Optional: Smooth the CT image (*e.g.* Gaussian blur)
2 Threshold the image keeping voxels of high intensity
3 From each 2D slice, remove objects that are smaller than a predefined area
4 Project the voxels of each slice to a 2D image along the Z-direction
5 Keep the largest connected region of the projection
6 Use the result of Step 5 as a binary mask and apply logical AND operation on each 2D slice
7 Make a copy of the image and dilate it
8 Keep the largest connected region of the dilated image
9 Classify connected objects from the image that fall outside of the result of Step 8 as "outliers"
10 Classify remaining object points as "bone" and all other voxels as "other object"

The approach may be fully automatized, though we suggest a semi-automatic extension if applicable. The segmentation result can be further improved by manually correcting the classification of misclassified parts (*e.g.* small bones farther away from the pelvis, contrast agent in the colon too close to the bone). We successfully applied this segmentation both for pelvic and thoracic studies.

B. Registration of pelvic and thoracic images

We tested our method on pelvic and thoracic data. We used the rigid-body restriction in our method and since the orientations of the objects are close to each other, it was enough to use only one initial orientation. We compared the results of our method against a classic intensity similarity method based on mutual information (MI) utilizing a multiresolution

pyramid scheme [11], that is adopted to binary objects[2]. Since ground truth is not known, we can perform visual inspection and compute the Dice coefficient as $\delta = \frac{|R \triangle O|}{|R| + |O|} \cdot 100\%$, where $\triangle$ denotes symmetric difference, while T, R and O are the sets of voxels of the *template*, *registered* object and *observation* respectively.

CT image pairs delineating the pelvic area were acquired at different times. The pairs of images were from the same patient. The spatial resolution of the CT studies were around $0.6-0.8$ mm in-slice. The slice distance was 5 mm in 11 cases, 2.5 mm in 4 cases. We also got three CT thoracic studies of the same person acquired by a PET-CT scanner. Here the in-slice resolution was 0.9766 mm and the slice distance was 3.27 mm. We used the full thoracic region and the extracted pelvis region also.

Our algorithm was implemented in Matlab 7.7 and was run on a desktop computer using Intel Core2 Duo processor at 2.4 GHz. The construction of the system of equations took around half a second, the optimization around 0.2 second. The average computing time of the MI method was around 2 minutes for the smaller, and 6 minutes for the larger pelvic CT studies. For the studies of the thorax, it usually took around 8 minutes to finish. This shows the clear advantage of our approach.

C. Pelvic CT results

The main challenges here are poor image resolution, substantial segmentation errors, and slightly different placement of the femoral head and lower portion of the spine. These CT experiments showed that even when the "identity criterion" required by our method is not fulfilled, the results are good or at least acceptable.

The MI method does provide lower δ-error values, and visually near perfect overlaps, see Figs. 2 and 3. Even these visually optimal cases produce quite high error values (always above 10%) incorporating the unknown segmentation errors. In few cases our method even outperforms the MI method. Very inaccurate segmentations (the real overlap between objects are above 20%) can produce higher δ errors, but usually such results still can be regarded as a fast, coarse approximations.

---

[2]Note that a simpler similarity metric could also be used here. *E.g.* the SSD (Sum of Squared Differences) metric could produce similar results requiring a bit less computing time.
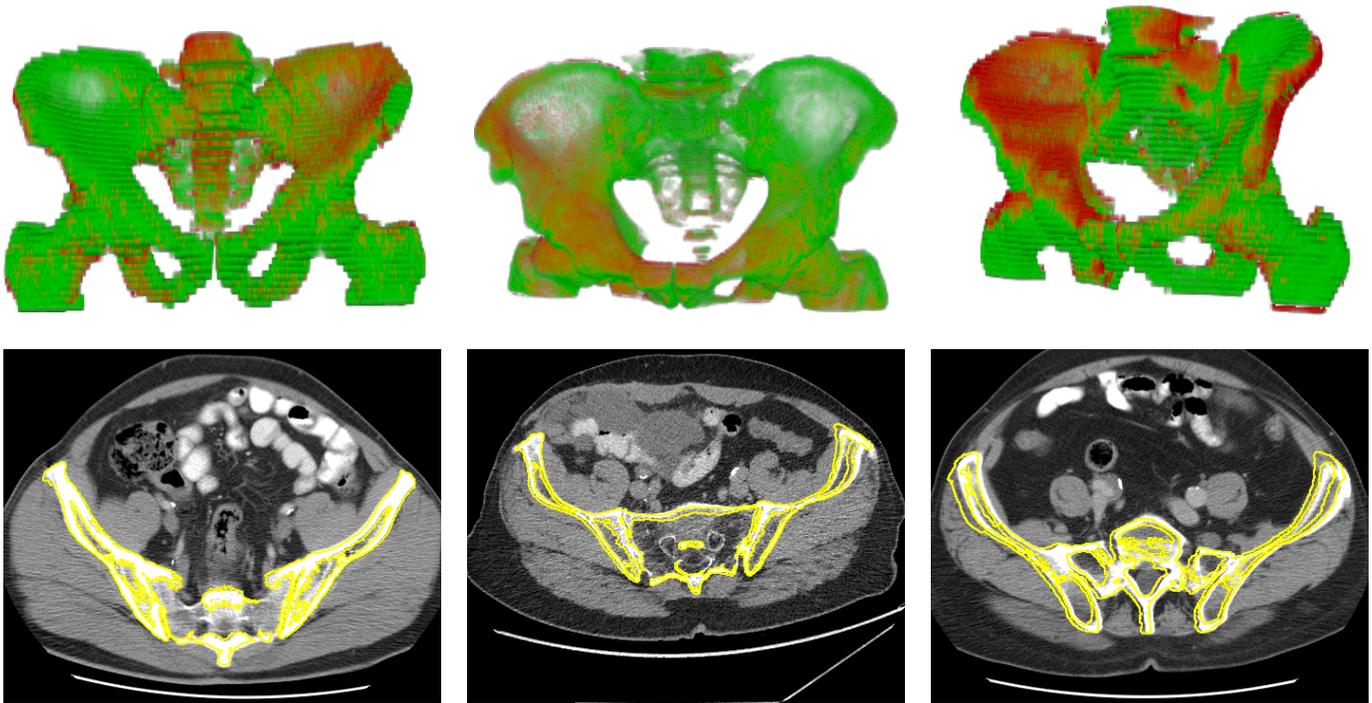
Fig. 3. Registration of pelvic CT data: superimposed registered 3D bone models (top row), and bone contours of the registered template (yellow) overlayed on a CT slice of the observations (bottom row). δ errors are 14.2%, 19%, and 27.87%. The first two cases show good alignment. Even the third one can be regarded as a fast, coarse approximation.

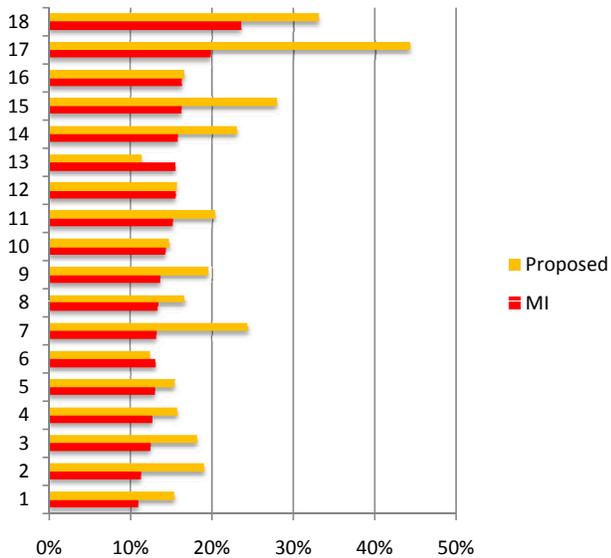Fig. 2. Registration results (δ-errors) of the pelvic CT tests ordered by best-to-worst errors of the MI method. Notice that even the best case exhibits quite large segmentation error (above 10%). Our method produces unacceptably high errors mainly when the segmentation error increases above 20%. The computing time is below 1 second in our case, while for the MI method it takes several minutes.
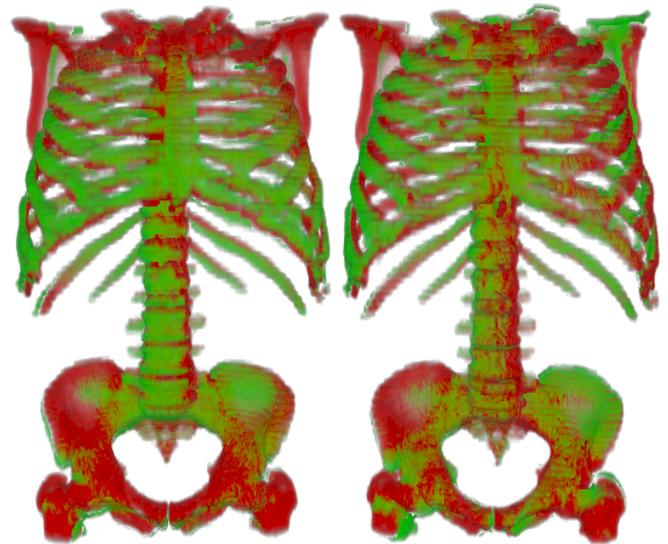

Fig. 4. Registration of thoracic CT data: superimposed registered 3D bone models. Perfect alignment is not possible due to the relative movements of the bone structure. Such a result is a good starting point for *e.g.* lymph node detection.

D. Thoracic CT results

For thoracic images the rigidity criterion no longer holds. Besides the femoral heads, the spine and the scapula can be moved with respect to each other. For such thoracic images both MI and our method provided errors above 30% (see Fig. 4). Still, such a result can be used as a good initialization for a lymph node pairing method.

IV. Conclusion

In this paper we extensively tested our registration method on real medical data. The solution is obtained by solving polynomial systems of equations, there is no need for further correspondences. Since our method has linear time complexity, it is especially suitable for fast and efficient registration of large images, even if the segmentations of the objects are not perfect. An optimized implementation could provide real-time registrations of 3D objects.

Acknowledgment

References

[1] R. Shams, P. Sadeghi, R. Kennedy, and R. Hartley, "A survey of medical image registration on multicore and the GPU," *IEEE Signal Processing Magazine*, vol. 27, no. 2, pp. 50–60, 2010.

[2] B. Zitová and J. Flusser, "Image registration methods: A survey," *Image and Vision Computing*, vol. 21, no. 11, pp. 977–1000, 2003.

[3] L. K. Ha, M. Prastawa, G. Gerig, J. H. Gilmore, C. T. Silva, and S. C. Joshi, "Image registration driven by combined probabilistic and geometric descriptors," in *Proceedings of Medical Image Computing and Computer-Assisted Intervention Part II*, 2010, pp. 602–609.

[4] P. Risholm, S. Pieper, E. Samset, and W. M. W. III, "Summarizing and visualizing uncertainty in non-rigid registration," in *Proceedings of Medical Image Computing and Computer-Assisted Intervention Part II*, 2010, pp. 554–561.

[5] L. Papp, M. Zuhayra, and E. Henze, "Semi-automatic epileptic hot spot detection in ECD brain SPECT images," in *Bildverarbeitung f´ur die medizin*, 2009, pp. 307–310.

[6] J. Zhang, Y. Ge, S. H. Ong, C. K. Chui, S. H. Teoh, and C. H. Yan, "Rapid surface registration of 3D volumes using a neural network approach," *Image and Vision Computing*, vol. 26, no. 2, pp. 201–210, 2008.

[7] J. Sterbis, K. Rice, M. Javitt, N. Schenkman, and S. Brassell, "Fusion imaging: A novel staging modality in testis cancer," *J Cancer*, pp. 223–229, 2010.

[8] P. Veit-Haibach, K. Strobel, and T. F. Hany, "New criteria refine PET/CT post-treatment follow-up," *Diagnostic Imaging Europe*, pp. 29–36, 2007.

[9] M. Kessler, "Image registration and data fusion in radiation therapy," *The British Journal of Radiology*, vol. 79, pp. S99–S108, 2006.

[10] N. D. Cornea, M. F. Demirci, D. Silver, A. Shokoufandeh, S. J. Dickinson, and P. B. Kantor, "3D object retrieval using many-to-many matching of curve skeletons," *Int. Conf. on Shape Modeling and Appl.*, pp. 368–373, 2005.

[11] J. Pluim, J. Maintz, and M. Viergever, "Mutual-information-based registration of medical images: a survey," *Medical Imaging*, vol. 22, no. 8, pp. 986–1004, 2003.

[12] A. Tanács, N. Sladoje, J. Lindblad, and Z. Kato, "Estimation of linear deformations of 3D objects," in *Proceedings of International Conference on Image Processing*, IEEE. Hong Kong, China: IEEE, September 2010, pp. 153–156.

[13] C. Domokos and Z. Kato, "Parametric estimation of affine deformations of planar shapes," *Pattern Recognition*, vol. 43, no. 3, pp. 569–578, 2010.

[14] A. Guimond, J. Meunier, and J. P. Thirion, "Average brain models: a convergence study," *Comput. Vision Image Understand.*, vol. 77, pp. 192–210, 2000.

[15] A. Tanacs, E. Mate, and A. Kuba, "Application of automatic image registration in a segmentation framework for pelvic CT images," in *Proceedings of CAIP*, ser. LNCS, vol. 3691, 2005, pp. 628–635.

[16] B. Ma, Z. Lin, S. Winkelbach, W. Lindenmaier, and K. Dittmar, "Automatic registration of serial sections of mouse lymph node by using Image-Reg," *Micron*, vol. 39, no. 4, pp. 387–396, 2008.